Electronic Supplementary Material (ESI) for Physical Chemistry Chemical Physics.

Electronic Supplementary Information

From Crystal to Glasslike Thermal Conductivity in Crystalline Minerals

Y. Bouyrie[1], C. Candolfi[1,*], S. Pailhès[2], M. M. Koza[3], B. Malaman[1], A. Dauscher[1], J. Tobola[4], O. Boisron[2], L. Saviot[5], B. Lenoir[1]

[1] *Institut Jean Lamour, UMR 7198 CNRS – Université de Lorraine, Parc de Saurupt, CS 50840, F-54011 Nancy, France*

[2] *Institute of Light and Matter, UMR 5306 Université Lyon 1-CNRS, Université de Lyon, F-69622 Villeurbanne cedex, France*

[3] *Institut Laue Langevin, 6 rue Jules Horowitz, B.P. 156, F-38042 Grenoble, Cedex 9, France*

[4] *Faculty of Physics and Applied Computer Science, AGH University of Science and Technology, 30–059 Krakow, Poland*

[5] *Laboratoire Interdisciplinaire Carnot de Bourgogne, UMR 6303 CNRS-Université de Bourgogne Franche-Comté, 9 avenue A. Savary, BP 47870, F-21078, Dijon Cedex, France*

Correspondence to: christophe.candolfi@univ-lorraine.fr

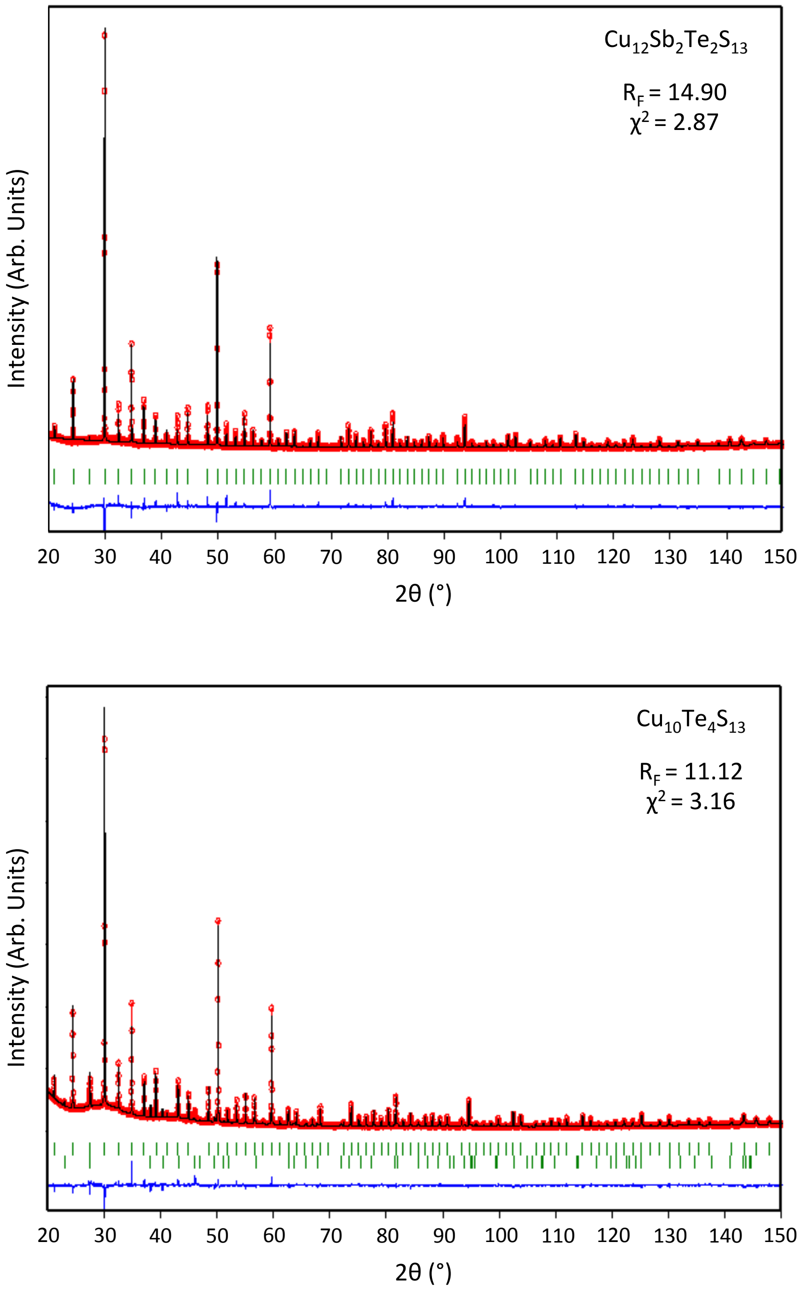

Fig. 1: Rietveld refinements of the PXRD patterns of $Cu_{12}Sb_2Te_2S_{13}$ and $Cu_{10}Te_4S_{13}$ tetrahedrites. The experimental data are shown by red open circles while the solid black line represents the calculated pattern. The lower blue line represents the difference between the experimental and calculated patterns. The green bars correspond to the Bragg reflections of the tetrahedrite phase (first row in the lower panel). For $Cu_{10}Te_4S_{13}$, the second row of green bars shows the expected reflections of elemental Te (4% mass estimated from refinements), which might hint at possible slight off-stoichiometry on the Cu and/or Te site. The lattice

parameters *a* are 10.35015(8) and 10.26468(9) Å for $Cu_{12}Sb_2Te_2S_{13}$ and $Cu_{10}Te_4S_{13}$, respectively.

Table 1: Atomic coordinates, site occupancies and equivalent atomic thermal displacement parameters (Å^2) of single crystalline $Cu_{10}Te_4S_{13}$ at 300K. The refined values of the anisotropic thermal displacement parameters are consistent with those inferred for the $Cu_{12}Sb_4S_{13}$ tetrahedrite by Pfitzner *et al.*[1]

Site	Atom	*x*	*y*	*z*	s.o.f	U_{11}	U_{22}	U_{33}	U_{23}	U_{13}	U_{12}
12*d*	Cu1	0.5	0	0.25	0.24427	0.0194(4)	0.0194(4)	0.0270(9)	0	0	0
12*e*	Cu2	0	0	0.21003(3)	0.16210	0.0276(7)	0.0276(7)	0.0143(1)	0	0	-0.0069(9)
8*c*	Te	0.26043(4)	0.26043(4)	0.26043(4)	0.16667	0.0132(1)	0.0132(1)	0.0132(1)	-0.0008(1)	-0.0008(1)	-0.0000(5)
24*g*	S1	0.88831(1)	0.88831(1)	0.35980(2)	0.5	0.0143(3)	0.0143(3)	0.0129(6)	-0.0029(3)	0.0029(3)	-0.011(5)
2*a*	S2	0	0	0	0.04167	0.0200(1)	0.0200(1)	0.0200(1)	0	0	0

Table 2: Atomic coordinates, site occupancies and equivalent atomic thermal displacement parameters (Å^2) of single crystalline $Cu_{12}Sb_2Te_2S_{13}$ at 300K.

Site	Atom	*x*	*y*	*z*	s.o.f	U_{11}	U_{22}	U_{33}	U_{23}	U_{13}	U_{12}
12*d*	Cu1	0.5	0	0.25	0.25	0.0192(3)	0.0192(3)	0.0256(5)	0	0	0
12*e*	Cu2	0	0	0.2168(3)	0.25	0.0737(1)	0.0737(1)	0.0185(1)	0	0	-0.052(1)
8*c*	Sb	0.26391(4)	0.26391(4)	0.26391(4)	0.1667	0.0124(2)	0.0124(2)	0.0124(2)	-0.0008(1)	-0.0008(1)	-0.0008(1)
24*g*	S1	0.8855(1)	0.8855(1)	0.3622(2)	0.5	0.0141(4)	0.0141(4)	0.0110(6)	0.001(4)	0.001(4)	-0.011(5)
2*a*	S2	0	0	0	0.04167	0.0174(1)	0.0174(1)	0.0174(1)	0	0	0

Table 3: Interatomic distances (in Å) and bond angles (in °) obtained from refinements of single-crystal XRD data at 300 K.

Composition	$Cu_{12}Sb_2Te_2S_{13}$	$Cu_{10}Te_4S_{13}$
Cu1 – S1 (×4)	2.33508	2.32346
Cu2 – S1 (×2)	2.25911	2.23380
Cu2 – S2	2.16048	2.15539
Cu2 – Cu2 (×4)	3.05538	3.04818
Cu2 – Sb/Te (×2)	3.47533	3.49009
Sb/Te – S1 (×3)	2.45991	2.38743
S1 – Cu1 – S1 (×2)	112.55	111.91
S1 – Cu2 – S1	91.24	93.05
S2 – Cu2 – S1 (×2)	134.38	133.48
Sb/Te – Cu2 – Sb/Te	170.48	170.03
S1 – Sb/Te – S1 (×3)	96.67	97.90

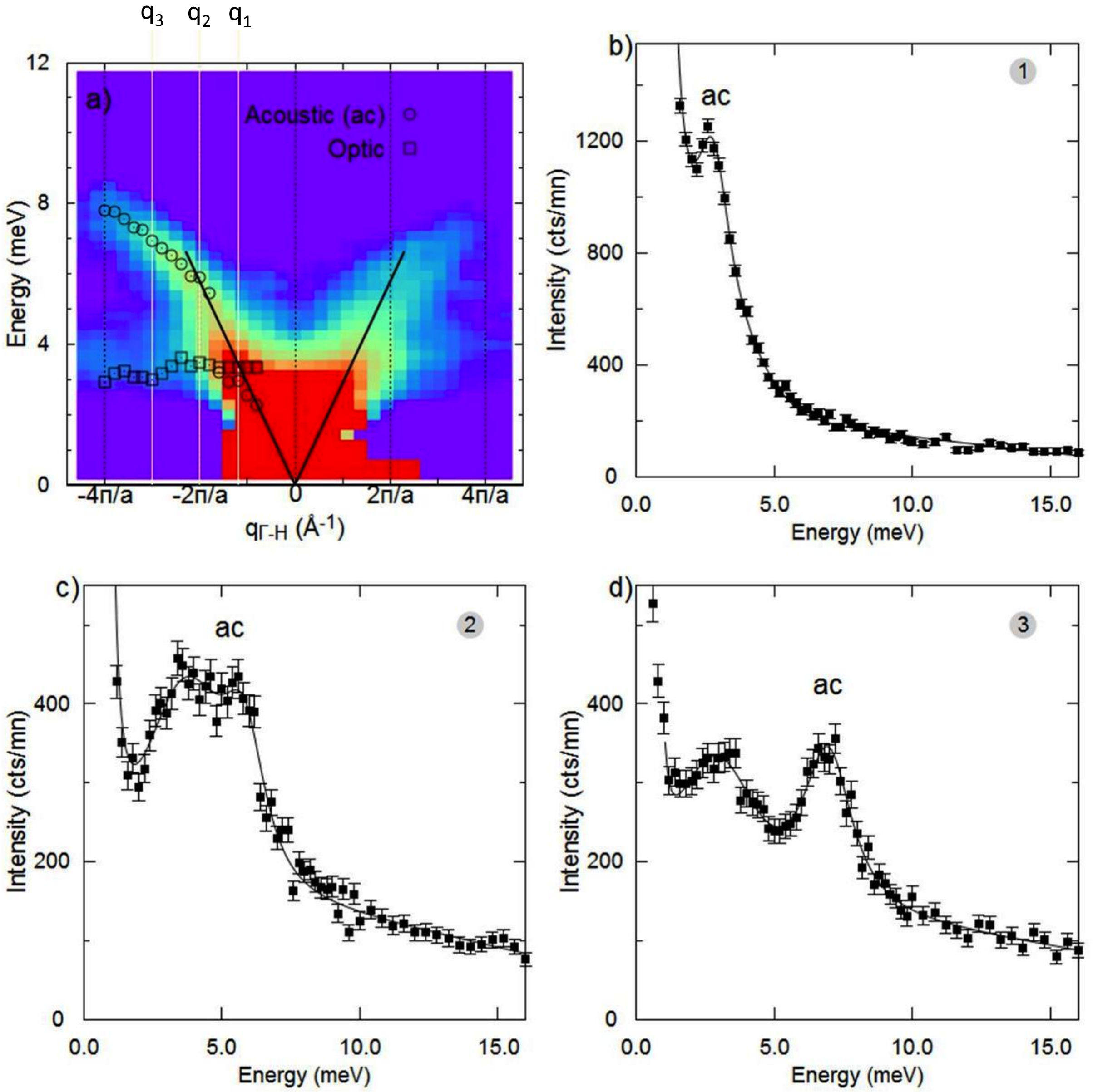

Figure 2. Mapping of the $\mathrm{TA}^{(100)}_{(011)}$ phonons measured in a natural, single-crystalline tetrahedrite specimen. a) Experimental neutron intensities represented as a false color image as a function of the wave vector and energy. Black open circles and squares represent the fitted experimental positions for the TA and optic phonons, respectively. The solid black line indicates the linear dispersion. **b)-d)** Raw data of constant energy scans performed at constant wave vectors $|q_1|=0.36$ (1), $|q_2|=0.61$ (2) and $|q_3|=0.91$ Å^{-1} (3). The measured scattering profiles were fitted using damped harmonic oscillators for acoustic phonons (labeled "ac" on the three figures) and Gaussian functions for the low-lying optical excitations.

X-ray Photoemission Spectroscopy (XPS)

The XPS experiments were performed at the ‘Plateforme Lyonnaise et Recherche sur les Agrégats (PLYRA)” on the two powdered tetrahedrites $Cu_{12}Sb_2Te_2S_{13}$ and $Cu_{10}Te_4S_{13}$. The data have been recorded at 300 K with a CLAM 4 vacuum generator (Al K line at 1486.6 eV). The photoelectrons were collected at pass energy of 10 eV in the fixed analyzer transmission mode giving a full-width at half maximum (FWHM) of 0.1 eV. The energy (position of the Fermi level) was calibrated by recording spectra from polycrystalline copper on the sample holder.

Electronic band structure calculations

The charge and spin self-consistent Korringa–Kohn–Rostoker Green’s function method was used to calculate the electronic structure of $Cu_{12}Sb_2Te_2S_{13}$ and $Cu_{10}Te_4S_{13}$ tetrahedrites.[2,3] The novel quasilinear algorithm was implemented to allow for more precise and less time consuming band structure calculations compared to conventional techniques.[4] The crystal potential of muffin-tin (MT) form was constructed within the local density approximation (LDA) framework using the Perdew-Wang formula for the exchange–correlation part.[5] The experimental values of lattice constants and atomic positions (Tables S1 and S2) were applied in all computations. For finally converged atomic charges (below $10^{-3}e$) and potentials (below 10 meV), the total, site-decomposed, and l-decomposed density of states (DOS) were computed using the integration tetrahedron method (~ 700 small tetrahedrons) in reciprocal space and 120 k-point grids in the irreducible part of the Brillouin zone.[6] The effects of chemical disorder on the electronic structure, namely Sb/Te alloying in $Cu_{12}Sb_{4-x}Te_xS_{13}$ (x = 0 and 2) and vacancy defects (on either Cu1 or Cu2 sites) in $Cu_{12-y}Te_4S_{13}$ (y = 0 and 2), have been studied employing the KKR method with the coherent potential approximation (CPA).[3] The CPA approach, which treats explicitly disorder as random, belongs to well-established techniques used to determine the electronic structure of intermetallic alloys. This approach does not require lowering the group symmetry of the unit cell in disordered systems thereby providing similar conditions of 'computational geometry' for different alloy compositions and end-points compounds. In KKR-CPA calculations, the CPA cycles have been performed self-consistently on the complex energy plane using an elliptic contour divided into 12 sections with four Gaussian quadrature points. The position of the Fermi level (E_F) was precisely determined from the generalized Lloyd formula. This enabled us to derive E_F precisely from the full derivative of the CPA Green's function without integrating over occupied states. This appears to be particularly important in systems close to metal – semiconductor transitions. In all figures presented herein, E_F is arbitrarily located at zero, and non-spin-polarized DOS curves are given in eV^{-1} per spin.

Active/Inert electronic lone pair

The XPS spectra of the valence band of $Cu_{12}Sb_2Te_2S_{13}$, shown in Figures S3a, exhibits a main peak with a maximum intensity located at a binding energy of – 3.2 eV followed by a tail that extends up to – 8 eV. This tail is further structured with two discernable peaks centred at about – 5 eV and – 7 eV. After the dip located above – 8 eV, a peak appears at – 14.2 eV. Below – 3.2 eV, a maximum in intensity is found at about – 1.4 eV.

The calculated total electronic density of states shown in Figure S3b reproduces well the overall shape of the XPS spectrum. A comparison between the partial density of states (Figure S3c) and this spectrum enables to assign the peak around – 14.2 eV to the *s*-states of the S, Sb and Te atoms. The main peak – 3.2 eV is mainly composed by the Cu *d*-states with slight contributions from the other atoms. The two peaks present in the tail may be mainly ascribed to the *p*-states of S1 and S2 atoms slightly shifted in energy.

Our calculations confirm that the 5*s*-states of Sb (Figure S3d), located at – 9 eV, shift towards lower binding energies for Te (found at – 11 eV). The *sp*-hybridization with the *p*-orbitals of S is therefore stronger with Sb than with Te resulting in a larger contribution of the *s*-states at energies close to the Fermi level (Figure S3e). This conclusion holds true in the $Cu_{10}Te_4S_{13}$ compound for which, the 5*s* states of Te are also located at – 11 eV (Figure S3f). While the lone pair of the Te atoms is thus inert, the stronger hybridization that arises in the case of Sb influences the force constants might play a role in governing the vibrational properties of the crystal.

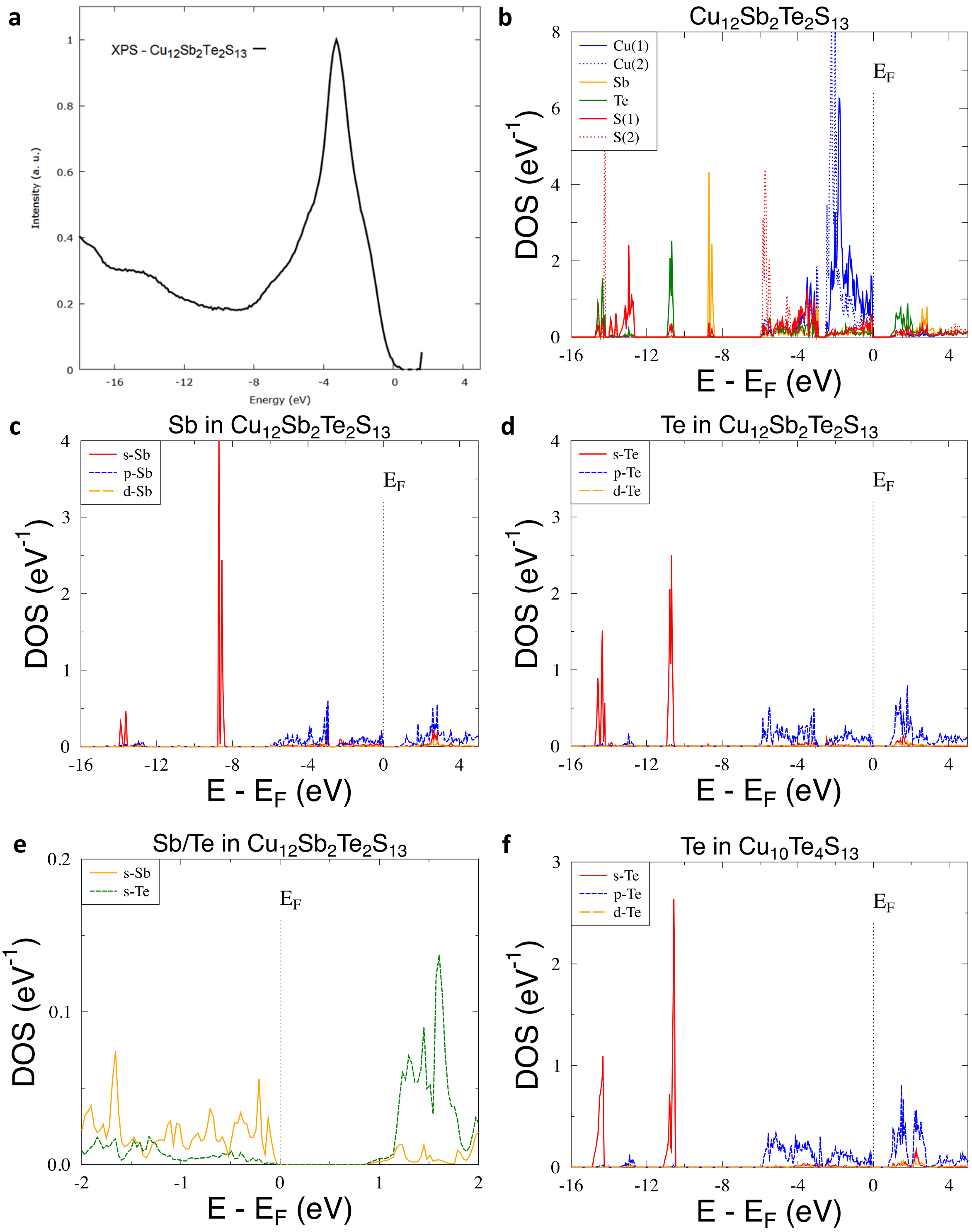

Figure 3. Total electronic density of states in the valence bands of $Cu_{12}Sb_2Te_2S_{13}$ measured by XPS **(a)** and calculated from KKR-CPA band structure calculations **(b)**. Panels **(c)** and **(d)** show the *l*-decomposed partial densities of states of the Sb and Te atoms. **(e)** Magnification of

the *s*-states contributions of the Sb and Te atoms near the Fermi level E_F. **(f)** *l*-decomposed density of states of Te in the Sb-free tetrahedrite.

References

1. A. Pfitzner, M. Evain and V. Petricek, *Acta Cryst.*, 1997, **B53**, 337.
2. A. Bansil, S. Kaprzyk, P. E. Mijnarends and J. Tobola, *Phys. Rev. B*, 1999, **60**, 13396.
3. T. Stopa, S. Kaprzyk and J. Tobola, *J. Phys.: Condens. Matter*, 2004, **16**, 4921.
4. S. Kaprzyk and P. E. Mijnarends, *J. Phys. C: Solid State Phys.*, 1986, **19**, 1283.
5. J. P. Perdew and Y. Wang, *Phys. Rev. B*, 1992, **45**, 13244.
6. S. Kaprzyk and A. Bansil, *Phys. Rev. B*, 1990, **42**, 7358.